

EXPRESS LETTER

Experimental Hamiltonian Learning of an 11-Qubit Solid-State Quantum Spin Register^{*}

To cite this article: P.-Y. Hou *et al* 2019 *Chinese Phys. Lett.* **36** 100303

View the [article online](#) for updates and enhancements.

Experimental Hamiltonian Learning of an 11-Qubit Solid-State Quantum Spin Register *

P.-Y. Hou(侯攀宇)[†], L. He(何丽)[†], F. Wang(王飞)[†], X.-Z. Huang(黄晔之), W.-G. Zhang(张文纲),
X.-L. Ouyang(欧阳晓龙), X. Wang(王歆), W.-Q. Lian(连文倩), X.-Y. Chang(常秀英),
L.-M. Duan(段路明)**

Center for Quantum Information, Institute for Interdisciplinary Information Sciences, Tsinghua University,
Beijing 100084

(Received 23 September 2019)

Learning the Hamiltonian of a quantum system is indispensable for prediction of the system dynamics and realization of high fidelity quantum gates. However, it is a significant challenge to efficiently characterize the Hamiltonian which has a Hilbert space dimension exponentially growing with the system size. Here, we develop and implement an adaptive method to learn the effective Hamiltonian of an 11-qubit quantum system consisting of one electron spin and ten nuclear spins associated with a single nitrogen-vacancy center in a diamond. We validate the estimated Hamiltonian by designing universal quantum gates based on the learnt Hamiltonian and implementing these gates in the experiment. Our experimental result demonstrates a well-characterized 11-qubit quantum spin register with the ability to test quantum algorithms, and shows our Hamiltonian learning method as a useful tool for characterizing the Hamiltonian of the nodes in a quantum network with solid-state spin qubits.

PACS: 03.67.-a

DOI: 10.1088/0256-307X/36/10/100303

Experimental realization of quantum registers is an essential task in quantum information processing (QIP). Lots of efforts towards this goal have been made on various systems such as trapped ions,^[1–3] solid-state spins,^[4–14] neutral atoms^[15] and superconducting qubits.^[16–19] One important system is the solid-state spin system associated with a single nitrogen vacancy (NV) center in a bulk diamond, which has been demonstrated to be a promising platform for quantum network,^[4–9] quantum computing,^[12,20] and quantum sensing.^[21–26] This system consists of one electron spin and multiple surrounding nuclear spins which are mostly provided by ¹³C atoms in the diamond lattice. It has been demonstrated that the electron spin could be initialized and detected by optical method, and manipulated with high fidelity by microwave signals.^[27,28] It is difficult to detect the surrounding nuclear spins directly, however, the dynamical decoupling (DD) technique has been well developed for universal control of nuclear spins,^[4,10–12,29–32] which is essentially realized by manipulating the electron spin with a DD sequence. Moreover, initialization and detection of nuclear spins can be implemented by a set of the DD-type gates.^[4,12,20] The electron spins of two remote NV centers can be entangled through photonic links,^[8,33,34] which leads to a promising path to a scalable quantum network based solid-state spin quantum register associated with NV centers in diamond.

In this solid-state spin register, it is worthwhile to

precisely characterize system Hamiltonian by learning the interaction parameters because: (1) the parameters of the DD-type nuclear spin gate are determined by the hyperfine interaction between the electron spin and the target nuclear spin, (2) the interactions among all the spin qubits are constantly on, so that it is inevitable to have crosstalk errors from the other nuclear spins while controlling the target nuclear spin. With the Hamiltonian parameters, dynamical decoupling sequence could be optimized to realize the desired operation on the target nuclear spin, in the mean time to reduce the gate errors due to unwanted crosstalk. In this work, we experimentally characterize the effective Hamiltonian of an NV center system composed of one electron spin and ten weakly coupled ¹³C nuclear spins. We first perform the DD spectroscopy to probe the surrounding spin environment which is realized by applying a DD sequence on the electron spin with a varying interpulse time. From the resulting DD spectrum, we identify 10 dominant nuclear spins which give strong signals to the electron spin coherence. We ignore the nuclear-nuclear interaction in this 11-qubit system because their strength is at least 1 order lower compared to electron-nuclear spin-spin interaction. Therefore, the essential Hamiltonian parameters are the parameters of the hyperfine interactions between the NV electron spin and each of the resolved 10 nuclear spins. We first roughly extract these hyperfine interaction parameters by fitting the simulated data to the experimental DD spectrum.

*Supported by the Frontier Science Center for Quantum Information of the Ministry of Education of China, Tsinghua University Initiative Scientific Research Program, and the National Key Research and Development Program of China (2016YFA0301902).

[†]They contributed equally to this work.

**Corresponding author. Email: lmduan@tsinghua.edu.cn

© 2019 Chinese Physical Society and IOP Publishing Ltd

Then, we precisely learn the hyperfine parameters of each nuclear spin by measuring the nuclear Larmor frequencies with different electron spin states. We apply an adaptive method^[35,36] based on the quantum phase estimation algorithm in a sequence of Ramsey-interferometry experiments to improve the efficiency of the frequency measurements. To validate the estimated Hamiltonian parameters, we numerically optimized quantum gates based on the learnt Hamiltonian parameters and experimentally implemented a universal set of quantum gates for this 11-qubit system.

We performed the experiments at a cryogenic temperature (~ 8 K) on a type-IIa CVD synthetic diamond sample with the natural abundance of ^{13}C ($\sim 1.1\%$). The 11-qubit system was composed of 1 NV electron spin $S = 1$ ($|m_s = 0\rangle \equiv |0\rangle, |m_s = \pm 1\rangle \equiv |\pm 1\rangle$) and 10 ^{13}C nuclear spins $I = 1/2$ ($|m_I = \frac{1}{2}\rangle \equiv |\uparrow\rangle, |m_I = -\frac{1}{2}\rangle \equiv |\downarrow\rangle$). The NV electron spin can be optically initialized with a fidelity over 99% through the intersystem crossing^[13] and read out in a single shot with an average fidelity of 90% ($F_0 = 81\%$ for $|0\rangle$ state and $F_1 = 99\%$ for $|\pm 1\rangle$ states) in Fig. 1(b). With a magnetic field B_z (~ 495 gauss) along the NV symmetry axis, the Hamiltonian of the 11-qubit system is described by

$$\hat{H} = D \cdot \hat{S}_z^2 + \gamma_e B_z \hat{S}_z + \sum_i (\hat{\mathbf{S}} \cdot \hat{\mathbf{A}}_i \cdot \hat{\mathbf{I}}_i + \gamma_n B_z \hat{I}_{i,z}), \quad (1)$$

where the NV symmetry axis is defined as the z axis. The electron (nuclear) spin operator $\hat{\mathbf{S}}$ ($\hat{\mathbf{I}}$) contains the Pauli matrices $\hat{S}_x, \hat{S}_y, \hat{S}_z$ ($\hat{I}_x, \hat{I}_y, \hat{I}_z$); D is the zero-field splitting of 2.8776 GHz; γ_e (γ_n) is the gyro-magnetic ratio of the electron spin (^{13}C nuclear spin); $\hat{\mathbf{A}}_i$ is the tensor of hyperfine interaction between the electron spin and the nuclear spin i . Dipole-dipole interactions between nuclear spins are typically negligible.

In the rotating frame defined by the Hamiltonian $H_0 = D\hat{S}_z^2 + \gamma_e B_z \hat{S}_z$, by neglecting the fast oscillation terms, we derive the effective Hamiltonian, which is described by

$$\begin{aligned} \hat{H}_{\text{eff}} = & \sum_i (A_{i,zx} \hat{S}_z \hat{I}_{i,x} + A_{i,zy} \hat{S}_z \hat{I}_{i,y} + A_{i,zz} \hat{S}_z \hat{I}_{i,z} \\ & + \gamma_n B_z \hat{I}_{i,z}) = \sum_i \hat{H}_i. \end{aligned} \quad (2)$$

In Eq. (2), the effective Hamiltonian \hat{H}_{eff} equals the sum of the subsystem Hamiltonians \hat{H}_i , which describes the hyperfine interaction between the electron spin and nuclear spin i . In particular, \hat{H}_i can be simplified to $\hat{H}_i = A'_{i,zx} \hat{S}_z \hat{I}_{i,x} + A'_{i,zz} \hat{S}_z \hat{I}_{i,z} + \gamma_n B_z \hat{I}_{i,z}$ by redefining the x axis for each nuclear spin so that $A'_{i,zy} = 0$ (the x, y axes for different nuclear spins can be defined independently as we have ignored the direct coupling terms between the nuclear spins). In the fol-

lowing, to simplify notation, we denote A'_{zz} and A'_{zx} in the rotated frame still as A_{zz} and A_{zx} by setting $A'_{zy} = 0$. Therefore, the main task of learning the whole system Hamiltonian is simplified as characterization of the hyperfine parameters $\{A_{zz}, A_{zx}\}$ for all the nuclear spins.

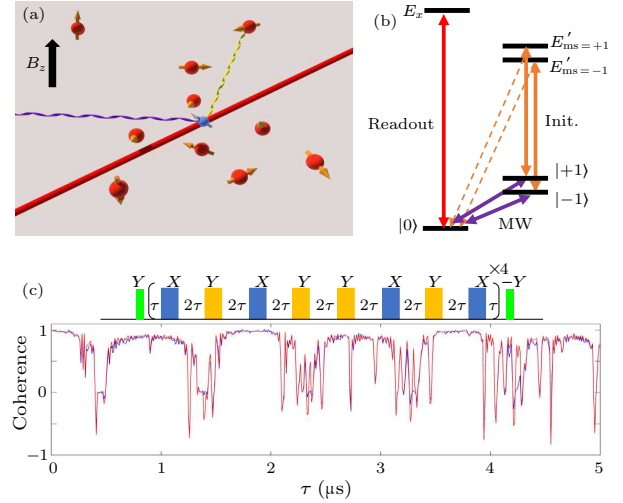


Fig. 1. (a) Illustration of an NV center system consisting of one electron spin (blue ball) and multiple nuclear spins (red balls). The electron spin is optically initialized and read out by the resonant laser (red line), manipulated by microwave fields (purple wave). (b) Diagram of relevant energy levels of the NV center, where $|0\rangle$ ($|\pm 1\rangle$) denotes respectively the bright (dark) state under a readout laser, and they are coherently manipulated by microwave signals. The state $|\pm 1\rangle$ can be optically pumped to $|0\rangle$ by an initialization laser. (c) Dynamical decoupling spectrum probed by the electron spin with a CPMG-32 pulse sequence. Blue and red lines denote the experimental data and the simulation results for the 10 resolved nuclear spins, respectively.

To explore the spin environment of an NV center, we prepared the electron spin in a superposition $(|0\rangle + |\pm 1\rangle)/\sqrt{2}$ with a $\pi/2$ pulse after optical initialization and applied a Carr-Purcell-Meiboom-Gill (CPMG) type of DD sequence with 32 π -pulses. The CPMG sequence was formed by $N = 32$ π -pulses with the configuration of $(\tau - \pi - \tau)^{\times N}$, where 2τ was the interval between two neighboring π -pulses. The phase of π -pulses in the CPMG sequence followed the XY-8 scheme shown in Fig. 1(c). The electron spin coherence was read out by projecting the final state on the x basis with a second $\pi/2$ pulse. By scanning pulse interval τ in the range of $0 < \tau < 50 \mu\text{s}$, we obtained the DD spectrum which was the electron spin coherence as a function of τ . Ten nuclear spins that gave strong coherence decay signals were resolved from the spectrum using the method in Ref. [11]. By fitting the simulation results to the experimental DD spectrum, the hyperfine parameters $\{A_{zz}, A_{zx}\}$ of 10 resolved nuclear spins were extracted with limited precision. This precision was limited because all the nuclear spins, in-

cluding the unresolved ones, contributed collectively to the DD spectrum, which made it hard to estimate the hyperfine parameters of each nuclear spin individually. However, these extracted hyperfine parameters, although with limited precision, still allowed us to perform quantum gates on the electron and nuclear spins with relatively low fidelities. With these gates, the 10 nuclear spins could be polarized with the fidelities ranging from 55% to 85%.

Nuclear spin Larmor precession frequency is affected by the hyperfine interaction with the electron spin. For a weakly coupled ^{13}C nuclear spin, f_{\pm} , defined as the precession frequency of the nuclear spin when the electron spin is in the $|\pm 1\rangle$ state, is given by

$$f_{\pm} = \frac{1}{2\pi} \sqrt{A_{zx}^2 + (A_{zz} \pm \omega_n)^2}, \quad (3)$$

where $\omega_n = \gamma_n B_z$. To precisely calibrate the parameters $\{A_{zz}, A_{zx}\}$ of each nuclear spin, we roughly polarized the target nuclear spin, and measured its precession frequency with the electron spin at $|+1\rangle$ and $|-1\rangle$ state. In this case, precision of $\{A_{zz}, A_{zx}\}$ was only determined by that of f_{\pm} , and was not affected by other nuclear spins, which were at fully mixed states so that they did not contribute to the measured signals.

To improve efficiency in measuring these precession frequencies,^[37] we implemented an adaptive quantum phase estimation algorithm. The basic idea of this adaptive scheme is to perform a sequence of Ramsey interferometry experiments with different precession time $t_n = 2^{N-n} t_{\min}$ ($n = 1, \dots, N$), so that the frequency probability distribution is updated after each Ramsey experiment and the frequency estimation range is gradually narrowed down. In each Ramsey experiment, the target nuclear spin is prepared into a superposition state $(|\uparrow\rangle + |\downarrow\rangle)/\sqrt{2}$ and the electron spin is prepared in the $|+1\rangle$ or $|-1\rangle$ state for measuring f_+ or f_- . Then, the target nuclear spin state freely evolves to $(|\uparrow\rangle + e^{i\phi_n} |\downarrow\rangle)/\sqrt{2}$ after t_n , where $\phi_n = 2\pi f t_n$ carries the information of the to-be-measured frequency f . Before the projective measurement of the nuclear spin along the x axis, a rotation $\hat{R}_Z^{\vartheta_n}$ along the z axis with an appropriate angle ϑ_n is applied on the nuclear spin to effectively change the measurement basis. Finally, the nuclear spin is measured with a probability $P_n = \frac{1 + \cos(\phi_n - \vartheta_n)}{2}$ in $|\uparrow\rangle$.

The essential idea of this method is to use P_n to update the frequency probability distribution by Bayesian inference and adaptively change the measurement basis based on the previous outcomes, i.e., to deduce the best rotation angle ϑ_{n+1} with $\{P_1, \dots, P_{n-1}\}$ for minimizing the uncertainty of P_{n+1} through the semiclassical implementation of the quantum phase estimation algorithm.^[37] After N -step Ramsey experiments, the frequency is estimated to be the value which gives the highest probability. The

to-be-measured frequency f can be represented with a binary digit form $f = \sum_{n=1}^N 2^n \cdot k_n \cdot f_0 + \varepsilon$ (see details in the Supplementary Material), where k_n equals 0 or 1 determining $P_n > 0.5$ or $P_n < 0.5$, $f_0 = \frac{1}{2t_{\max}}$ is the measured precision with t_{\max} representing the longest precession time of nuclear spin, and $\varepsilon < f_0$ represents the error term.

We performed the Ramsey interferometry experiments sequentially with precession time $t_n = 2^{N-n} t_{\min}$ ($n = 1, \dots, N$), so that k_n was updated one by one, starting from the least significant digit. Each Ramsey experiment was repeated 1000 times. The angle of the Z-rotation gate was updated with $\vartheta_{n+1} = \frac{\vartheta_n}{2} + \frac{k_n \pi}{2}$ starting with the initial phase $\vartheta_1 = \frac{\pi}{2}$. In the experiment, we chose $t_{\min} = 800$ ns to make sure ϕ_n within $(0, \pi]$. The maximal time $t_{\max} = 2^{N-1} t_{\min}$ was determined by the nuclear spin coherence time which is typically around 10 ms. Figure 2(c) shows an example of the frequency estimation result. Here k_n (red circles) were estimated to be 0 or 1 determined by $P_n > 0.5$ or $P_n < 0.5$. By adaptively changing the measurement basis, P_n moved away from 0.5 (k_n approaches 0 or 1) in the quantum phase estimation algorithm, but eventually it was limited by the nuclear spin polarization fidelity. For the first Ramsey experiment, P_0 was measured to be near 0.5 because of no adaptive change of the basis before this measurement and a significant decoherence during the long precession time.

Two major imperfections affected the precision in measurement of the precession frequency: (i) nuclear spin decoherence, (ii) magnetic field misalignment. Limited by the first kind of imperfection, we chose t_{\max} to be smaller than nuclear spin coherence time. To suppress the influence of the second kind, we calibrated the transverse magnetic field B_x to be near zero by minimizing the sum of the two electron spin resonant frequencies $f_{|0\rangle \leftrightarrow |\pm 1\rangle}$. However, the intrinsic short coherence time of the electron spin led to a wide resonance linewidth so that B_x could only be calibrated to be smaller than 2.5 gauss. The residual B_x field could cause a fairly large error in the nuclear spin precession frequency, which was estimated by the form

$$\Delta f_{\pm} \approx \frac{(A_{zz} \pm \omega_n) A_{zx} \omega_{ex}}{f_{\pm} (D \pm \omega_e)} \pm \frac{A_{zx} \omega_{nx}}{f_{\pm}}, \quad (4)$$

where $\omega_{ex} = \gamma_e B_x$, $\omega_{nx} = \gamma_n B_x$ (see details in the Supplementary Material).

Hyperfine parameters A_{zz}, A_{zx} of the resolved nuclear spins were calculated by Eq. (3) and (4), and listed in Table 1. With this precisely calibrated hyperfine parameters, we numerically simulated the DD spectrum and compared the simulation results with the experimental data. In Fig. 1(c), the simulation results coincided with most of the signals in the spectrum, and the deviations in certain regions were caused by the unresolved nuclear spin bath.

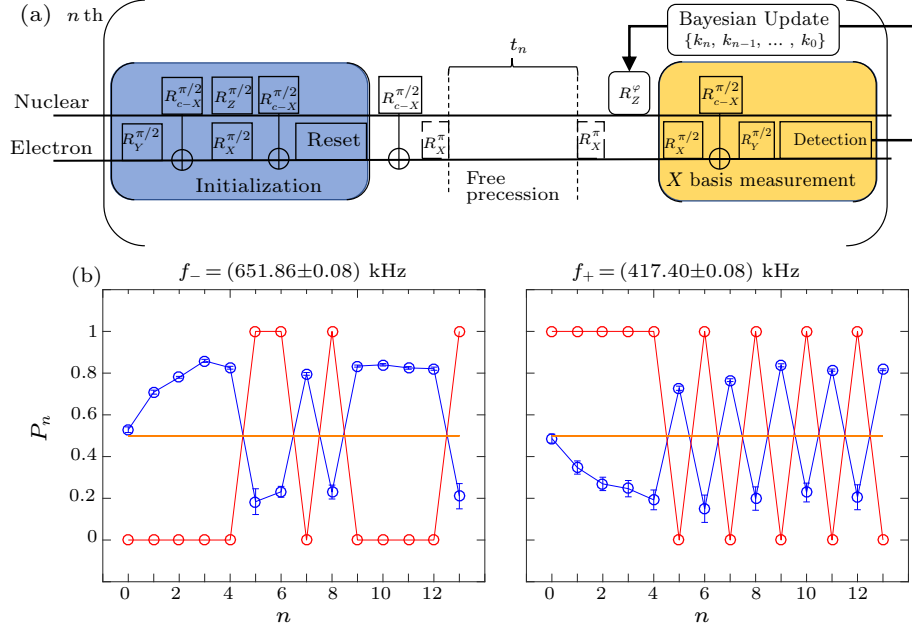


Fig. 2. (a) Experimental sequence to measure the nuclear spin precession frequency under different states of the electron spin through an adaptive method based on the quantum phase estimation algorithm. (b) Frequency measurement results of f_- (left panel) and f_+ (right panel). In the n th Ramsey experiment, k_n (red circle) is estimated by the corresponding outcome of probability P_n (blue circles with the error bar).

Table 1. Measured nuclear spin hyperfine parameters and initialization fidelities. The number in the bracket denotes the error bar in the last digit.

No.	1	2	3	4	5
A_{zx} (kHz)	208(1)	72(1)	72(1)	71(1)	43(1)
A_{zz} (kHz)	566.0(3)	45.9(1)	-15.1(1)	118.1(1)	5.50(7)
F_{init} (%)	95(2)	94(1)	93(1)	97(1)	92(1)
No.	6	7	8	9	10
A_{zx} (kHz)	33(1)	32(1)	31(1)	29(1)	17(1)
A_{zz} (kHz)	-49.64(5)	46.34(5)	27.09(5)	28.70(5)	-14.28(3)
F_{init} (%)	93(1)	81(1)	78(1)	78(1)	86(1)

With the precisely characterized parameters, we designed a universal set of quantum gates for this 11-spin register by simulation, including the single-qubit gates ($\hat{R}_X^{\pi/2}$, $\hat{R}_Z^{\pi/2}$, $\hat{R}_Z^{\pi/4}$ with subscript and superscript representing rotation axis and angle respectively) for each electron and nuclear spin, and the controlled rotation gates ($\hat{R}_{c-X}^{\pi/2}$ with electron spin the controlling qubit) between the electron and each nuclear spin. To eliminate crosstalk caused by the constantly-on interactions between electron and other nuclear spins, we numerically optimized the target gate sequence by taking into account the Hamiltonian of other resolved nuclear spins. In addition, to model the unresolved nuclear spins, we randomly chose 10 additional nuclear spins with the interaction parameters uniformly distributed in the range $|A_{zz}, A_{zx}| < 10$ kHz (this range was reasonable as for nuclear spins with larger hyperfine parameters, they should have been identified already) in the simulation. Nuclear spin single-qubit gates were designed by minimizing gate duration to mitigate the decoherence effect. Controlled entan-

gling gates $\hat{R}_{c-X}^{\pi/2}$ were optimized by minimizing the crosstalk to other nuclear spins.

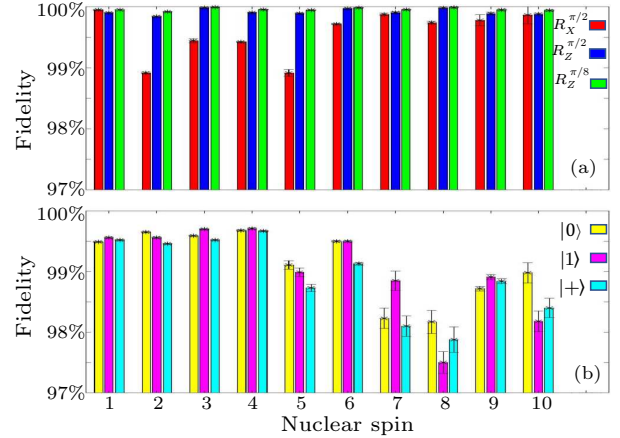


Fig. 3. Histogram of estimated gate fidelities for the 10 resolved nuclear spins. (a) Estimated gate fidelities of single-qubit gates $\hat{R}_X^{\pi/2}$, $\hat{R}_Z^{\pi/2}$, $\hat{R}_Z^{\pi/4}$ for each nuclear spin. (b) The fidelities of the entangling gates $\hat{R}_{c-X}^{\pi/2}$ between the electron spin and each nuclear spin under different initial states $|e \uparrow\rangle$, $|e\rangle = |0\rangle, |1\rangle, |+\rangle$ for the control qubit (electron spin). The gate fidelities are estimated through fit to the decay of the state fidelity under repeated application of the same gates.

In the experiment, we used these optimized nuclear spin gate parameters from simulation to polarize the resolved nuclear spins with fidelities shown in Table 1. The fidelities were significantly improved compared with that when we had only a rough estimation of the hyperfine interaction parameters through the DD spectrum. To evaluate the learnt hyperfine param-

ters, we applied a calibration method^[38,39] to estimate the errors of the gates derived from these hyperfine parameters, in which overall state fidelity decays were investigated by repeatedly applying same gates on a certain initial state. By using this method, we could only get the partial information of the gate errors and obtained gate fidelities which were likely higher than the actual gate fidelities, because some unitary errors could be canceled by repeating the gate. However, it gave a rough indicator of the gate fidelity and was sufficient for validating the learnt hyperfine parameters. To analyze single-qubit gate error, we polarized nuclear spins to the $|\uparrow\rangle$ state and applied the same gate M times so that the net operation was an identity, and measured the state fidelity between the outcome state and the ideal target state. The gate fidelity F_{gate} was deduced by fitting the state fidelity decay $F_{\text{state}}(M)$ with a linear function $F_{\text{state}} = F_{\text{init}} - M \cdot F_{\text{gate}}$, where F_{init} was the nuclear spin initialization fidelity. To eliminate the potential bias in the electron initialization state, we repeated the experiments with electron spin in $|0\rangle$ and $|-1\rangle$ state respectively. Final gate fidelities shown in Fig. 3(a) were estimated with the average value of the two cases.

Analogous to single-qubit gate fidelity estimation, we also estimated the fidelity of the two-qubit entangling gate $\hat{R}_{c-X}^{\pi/2}$ by measuring the electron-nuclear spin joint state fidelity. We prepared the electron spin in $|0\rangle$, $|-1\rangle$ and $|+\rangle = (|0\rangle + |-1\rangle)/\sqrt{2}$ states, respectively, and showed the corresponding results in Fig. 3(b). Each nuclear spin was initialized to the $|\uparrow\rangle$ state. The results indicated that the two-qubit gate $\hat{R}_{c-X}^{\pi/2}$ fidelities of the strongly coupled nuclear spins with strong hyperfine interaction strength were higher than that of weakly coupled nuclear spins. It implied that the spin bath still introduced crosstalk error to the gate operations of the resolved nuclear spins and the weakly coupled nuclear spins suffered more crosstalk to the spin bath than the strongly coupled ones.

In summary, we have experimentally learnt the effective Hamiltonian of an 11-qubit solid-state quantum spin register in a diamond NV center. The learning of the Hamiltonian parameters was implemented by combining the rough parameter estimation from the DD spectrum and the precise determination of each parameter through the adaptive measurement of the nuclear spin precession frequency with the semiclassical quantum phase estimation algorithm. As an example application of the learnt multi-qubit interaction Hamiltonian with precisely determined parameters, we designed and optimized a universal set of quantum gates on these 11 spin qubits under the constantly-on interaction and used the knowledge of the learnt interaction parameters to minimize the crosstalk errors. In future, we could implement longer

dynamical decoupling sequences to identify other more weakly coupled nuclear spins from the spin bath. This knowledge would help to further improve the initialization and the gate fidelities for those weakly coupled nuclear spins and reduce the crosstalk error between them. Some of the Hamiltonian learning techniques adopted here, such as the two-step protocol and the adaptive quantum phase estimation algorithm, may also find applications in other multi-qubit systems to characterize the full interaction Hamiltonian and to minimize the crosstalk errors for quantum gate operations.

Note Added: After completion of this work, we became aware of a related work^[40] that demonstrated a universal set of quantum gates in a 10-qubit quantum spin register.

Data Availability: The data that support the findings of this study are available from the authors upon request.

Competing Interests: The authors declare that there are no competing interests.

Author Information: Correspondence and requests for materials should be addressed to L.M.D. (lmd-uan@tsinghua.edu.cn).

Author Contributions: L.M.D. proposed the experiment and supervised the project. P.Y.H., F.W., X.Z.H., W.G.Z., X.L.O., X.W., X.-Y. Chang carried out the experiment. L.H. and W.Q.L. prepared the diamond sample. P.Y.H., L.H. and F.W. contribute equally to this experiment. P.Y.H., L.M.D., F.W. wrote the manuscript.

References

- [1] Monz T, Schindler P, Barreiro J T, Chwalla M, Nigg D, Coish W A, Harlander M, Hansel W, Hennrich M and Blatt R 2011 *Phys. Rev. Lett.* **106** 130506
- [2] Friis N, Marty O, Maier C, Hempel C, Holzappel M, Jurcevic P, Plenio M B, Huber M, Roos C, Blatt R 2018 *Phys. Rev. X* **8** 021012
- [3] Zhang J, Pagano G, Hess P W, Kyprianidis A, Becker P, Kaplan H, Gorshkov A V, Gong Z X and Monroe C 2017 *Nature* **551** 601
- [4] Reiserer A, Kalb N, Blok M S, K J van Bemmelen, Taminiau T H, Hanson R, Twitchen D J and Markham M 2016 *Phys. Rev. X* **6** 021040
- [5] Humphreys P C, Kalb N, Morits J P, Schouten R N, Vermeulen R F, Twitchen D J, Markham M and Hanson R 2018 *Nature* **558** 268
- [6] Childress L and Hanson R 2013 *MRS Bull.* **38** 134
- [7] Dutt M G, Childress L, Jiang L, Togan E, Maze J, Jelezko F, Zibrov A, Hemmer P and Lukin M 2007 *Science* **316** 1312
- [8] Pfaff W, Hensen B, Bernien H, S B Van Dam, Blok M S, Taminiau T H, Tiggelman M J, Schouten R N, Markham M, Twitchen D J 2014 *Science* **345** 532
- [9] S B Van Dam, Humphreys P C, Rozpkedek F, Wehner S and Hanson R 2017 *Quantum Sci. Technol.* **2** 034002
- [10] Abobeih M H, Cramer J, Bakker M A, Kalb N, Markham M, Twitchen D and Taminiau T H 2018 *Nat. Commun.* **9** 2552
- [11] Taminiau T H, Wagenaar J J T, T van der Sar, Jelezko F,

- Dobrovitski V V and Hanson R 2012 *Phys. Rev. Lett.* **109** 137602
- [12] Taminiau T H, Cramer J, T van der Sar, Dobrovitski V V and Hanson R 2014 *Nat. Nanotechnol.* **9** 171
- [13] Goldman M L, Sipahigil A, Doherty M W, Yao N Y, Bennett S D, Markham M, Twitchen D J, Manson N B, Kubanek A and Lukin M D 2015 *Phys. Rev. Lett.* **114** 145502
- [14] Casanova J, Wang Z Y and Plenio M B 2017 *Phys. Rev. A* **96** 032314
- [15] Bernien H, Schwartz S, Keesling A, Levine H, Omran A, Pichler H, Choi S, Zibrov A S, Endres M, Greiner M 2017 *Nature* **551** 579
- [16] Kelly J, Barends R, Fowler A G, Megrant A, Jeffrey E, White T C, Sank D, Mutus J Y, Campbell B, Chen Y 2015 *Nature* **519** 66
- [17] *Ibm makes quantum computing available on ibm cloud*
- [18] Song C, Xu K, Li H, Zhang Y R, Zhang X, Liu W, Guo Q, Wang Z, Ren W, Hao J 2019 *Science* **365** 574
- [19] Yan Z, Zhang Y R, Gong M, Wu Y, Zheng Y, Li S, Wang C, Liang F, Lin J, Xu Y 2019 *Science* **364** 753
- [20] Cramer J, Kalb N, Rol M A, Hensen B, Blok M S, Markham M, Twitchen D J, Hanson R and Taminiau T H 2016 *Nat. Commun.* **7** 11526
- [21] Maletinsky P, Hong S, Grinolds M S, Hausmann B, Lukin M D, Walsworth R L, Loncar M and Yacoby A 2012 *Nat. Nanotechnol.* **7** 320
- [22] Schirhagl R, Chang K, Loretz M and Degen C L 2014 *Annu. Rev. Phys. Chem.* **65** 83
- [23] Lovchinsky I, Sushkov A O, Urbach E, N P de Leon, Choi S, K De Greve, Evans R, Gertner R, Bersin E, Muller C 2016 *Science* **351** 836
- [24] Boss J M, Cujia K S, Zopes J and Degen C L 2017 *Science* **356** 837
- [25] Schmitt S, Gefen T, Stürner F M, Unden T, Wolff G, Müller C, Scheuer J, Naydenov B, Markham M, Pezzagna S 2017 *Science* **356** 832
- [26] Degen C L, Reinhard F and Cappellaro P 2017 *Rev. Mod. Phys.* **89** 035002
- [27] Dolde F, Bergholm V, Wang Y, Jakobi I, Naydenov B, Pezzagna S, Meijer J, Jelezko F, Neumann P, Schulte-Herbrüggen T 2014 *Nat. Commun.* **5** 3371
- [28] Arroyo-Camejo S, Lazarev A, Hell S W and Balasubramanian G 2014 *Nat. Commun.* **5** 4870
- [29] G De Lange, Wang Z, Riste D, Dobrovitski V and Hanson R 2010 *Science* **330** 60
- [30] Naydenov B, Dolde F, Hall L T, Shin C, Fedder H, Hollenberg L C L, Jelezko F and Wrachtrup J 2011 *Phys. Rev. B* **83** 081201
- [31] Pham L M, Bar-Gill N, Belthangady C, D Le Sage, Cappellaro P, Lukin M D, Yacoby A and Walsworth R L 2012 *Phys. Rev. B* **86** 045214
- [32] Liu G Q, Po H C, Du J, Liu R B and Pan X Y 2013 *Nat. Commun.* **4** 2254
- [33] Bernien H, Hensen B, Pfaff W, Koolstra G, Blok M, Robledo L, Taminiau T, Markham M, Twitchen D, Childress L 2013 *Nature* **497** 86
- [34] Kalb N, Reiserer A A, Humphreys P C, Bakermans J J, Kamberling S J, Nickerson N H, Benjamin S C, Twitchen D J, Markham M and Hanson R 2017 *Science* **356** 928
- [35] Bonato C, Blok M S, Dinani H T, Berry D W, Markham M L, Twitchen D J and Hanson R 2016 *Nat. Nanotechnol.* **11** 247
- [36] Cappellaro P 2012 *Phys. Rev. A* **85** 030301
- [37] Griffiths R B and Niu C S 1996 *Phys. Rev. Lett.* **76** 3228
- [38] Zu C, Wang W B, He L, Zhang W G, Dai C Y, Wang F and Duan L M 2014 *Nature* **514** 72
- [39] Rong X, Geng J, Shi F, Liu Y, Xu K, Ma W, Kong F, Jiang Z, Wu Y and Du J 2015 *Nat. Commun.* **6** 8748
- [40] Bradley C E, Randall J, Abobeih M H, Berrevoets R C, Degen M J, Bakker M A, Markham M, Twitchen D J and Taminiau T H 2019 *Phys. Rev. X* **9** 031045